Replacing the detector mask with a structured scintillator in edge-illumination x-ray phase contrast imaging

Lorenzo Massimi[a,†,*], Gibril K. Kallon[a], Ian Buchanan[a], Marco Endrizzi[a], Piotr Dobrosz[b], Rob Brooks[c], Daniel Brau[c], Ed Bullard[b,‡], and Alessandro Olivo[a]

[a]Department of Medical Physics and Biomedical Engineering, University College London, London, UK
[b]Scintacor Ltd, 125 Cowley Road, Cambridge CB4 0DL, UK
[c]Photonic Science and Engineering Ltd, 22 Theaklen Drive, Saint Leonards-on-sea TN38 9AZ, UK
[†]Current address: Institute of Nanotechnology, National Research Council, Rome, Italy
[‡]Current address: ISDI Ltd, Highgate Business Centre, 33 Greenwood Place, London NW5 1LB, UK
[*]Corresponding author. Email: l.massimiphd@gmail.com

May 9, 2022

Abstract

We present a proof-of-concept Edge Illumination X-Ray Phase Contrast system where the detector mask has been replaced by an indirect conversion detector in which sensitive and insensitive regions have been obtained by "patterning" the scintillator. This was achieved by creating a free-standing grid with period and aperture size matching that of a typical detector mask, and filling the apertures with gadolinium oxysulfide. Images of various samples were collected with both the modified and the original edge illumination systems based on the use of two masks to characterize the performances of this detector design. We found that, despite the proof-of-concept nature of this attempt resulting in a structured detector with suboptimal performance, it allows effective separation of the attenuation and refraction channels through phase retrieval, and the visualization of hard-to-detect features such as cartilage through the latter channel, thus demonstrating that the proposed approach holds the potential to lead to improved stability since it will use a single optical element facilitating the design of rotating phase contrast systems, or the retrofitting of conventional x-ray systems.

1 Introduction

Thanks to the availability of the highly brilliant and coherent X-ray beams provided by synchrotron radiation facilities, the interest in X-ray phase-based methods has increased significantly. Phase-based methods allow overcoming the low contrast of conventional X-ray imaging when imaging soft tissues [1,2]. This is an intrinsic limitation due to image formation being based on the difference in the absorption coefficients, which is usually small between soft tissues. Conversely, phase contrast imaging is based on the use of the real part of the complex refractive index δ, referred to as phase coefficient, that describes the phase shift experienced by an electromagnetic wave when passing through a material. Images generated by exploiting phase shifts were shown to provide a higher contrast for soft tissues and have been proven to be extremely valuable in preclinical studies, allowing the detection and quantification of otherwise invisible features [3,4,5,6]. Since having to rely on synchrotrons limited a widespread use of the technique [7], approaches working with conventional sources have been developed [8,9]. The availability of such techniques represented the first necessary step towards the translation into clinical practice and allowed the investigation of a large number of pre-clinical applications in standard labs [10,11,12]. Most of these techniques are based on optical elements. Among these, edge illumination (EI) was demonstrated to achieve a relatively low dose as well as to cover large fields of views [8,13,14]. It is based on the use of two absorption masks, the first placed in front of the sample and the second in contact with the detector. While it has been shown that it is not required to precisely align the two masks to obtain high-quality phase contrast images [15], the second (detector) mask still needs to be accurately

aligned with the pixel lattice of the underlying detector. This is a critical requirement, with misalignment of the detector mask affecting the phase sensitivity of an EI system. In order to remove this limitation, in this manuscript we present the first proof-of-concept that detector mask and relative alignment can be eliminated by embedding its function directly in the X-ray scintillator. Free-standing microstructures with a period matching that of a standard detector used in EI and apertures corresponding to 40% of the period were fabricated. These apertures were filled with scintillator powder (Gadox, Gadolinium Oxysulfide) and mounted directly on a sensor. The resulting sensor corresponds to a standard, aligned "detector plus detector mask" configuration in EI, with the Gadox-filled apertures providing regular sensitive areas separated by insensitive, Gadox-free septa. To test its performance, the structured detector obtained as described above has been implemented into an EI system. Its quantitative response has been investigated by imaging plastic wires of different materials and comparing the results both with theoretical profiles and with the results obtained with a conventional EI system using a flat panel detector and a detector mask. This showed that the structured detector allows for a reliable separation of the transmission and refraction contrast channels. Image quality is poorer than that obtained with the standard EI system, mainly because of the yet nonoptimized manufacturing process which led to an excessive height and a significant non-uniformity of the deposited scintillator layer. Indeed, we deliberately kept the structures higher than the amount of scintillator needed for an optimised detector response at the considered energy range (40 kVp molybdenum spectrum), because for this first proof-of-concept experiment we did not know what sort of filling efficiency we could expect and we wanted to ensure the achievement of a detectable signal. However, when used to image a bone sample, the EI system based on the structured detector allowed for a straightforward visualisation of the cartilage layer (invisible in conventional transmission), providing results comparable with those obtained with the flat panel. While the manufacturing process still needs significant optimization, this demonstrates that a system based around a structured scintillator concept can in principle be used for medical applications. Once optimised, this could lead to a system with improved stability and utilising a single optical element, which would facilitate the design of rotating phase contrast systems, or the retrofitting of conventional x-ray systems. Furthermore, the system's cost and complexity would be significantly reduced. Finally, we note that structured scintillators were previously proposed to enhance the MTF of x-ray detectors or, with a similar aim to that pursued in this paper, to eliminate the analyser grating in grating interferometry [16,17]. This paper presents the first application to an EI system; as a consequence, it also involves the development of structures on a significantly different scale.

2 Methods

2.1 Structured detector

Free-standing grating structures with a period of 50 μm and regular, long parallel 20 μm apertures were fabricated by Microworks GmbH (Karlsruhe, Germany). Structures were fabricated in two materials, a silver coated polymer and gold. The latter was used in the experiments described in this paper, because the silver coating was observed to chip away during dicing and subsequent manipulation of the structures. The free-standing gold structure was glued to the top of a fibre-optic plate by spin-coating a thin layer of epoxy resin, which also helped keeping it perfectly flat for scintillator filling and subsequent imaging. This was immersed with the structure on top in an aqueous solution of Gadox plus binder, allowing for the scintillator particles to deposit as water evaporates. The process was repeated a few times until the apertures appeared entirely filled, and the excess Gadox gently removed. To be sure to obtain a detectable signal in every aperture, we aimed to produce a 300 μm thick Gadox layer by using free-standing grating structures of the same height. This thickness is significantly higher than that of a Gadox screen that would normally be used with a 40 keV molybdenum beam (see below). Subsequent data analysis showed that most of this thickness was actually filled, albeit in a non-uniform way, resulting in suboptimal energy response due to the re-absorption of the generated optical photons. However, it enabled us to obtain the desired proof-of-concept results. While the structured scintillator obtained in this manner would be a match to a 50 micron pixel sensor, this was not available at the time this experiment was conducted. It was therefore mounted on a Photonics Science XR FDS CCD camera with a 4.5 μm pixel size, and pixels were appropriately binned post-acquisition to simulate a 50 μm pixel detector , allowing a direct comparison with the results obtained with the flat panel which represents our standard.

2.2 Experimental setup

Two different EI setups have been used, a conventional one featuring two masks and a flat panel detector as used in previous work, and a single (sample) mask one using the CCD camera with the structured scintillator [18]. Both are "compact" setups which follow the design recently implemented for intra-operative specimen

imaging[19,20], resulting from the previous demonstration that reducing the system length at constant magnification does not negatively affect the (phase) signal-to-noise ratio if the exposure time is kept constant[21]. Schemes of these systems are shown in Fig.1. A conventional EI system is based on the use of two absorption

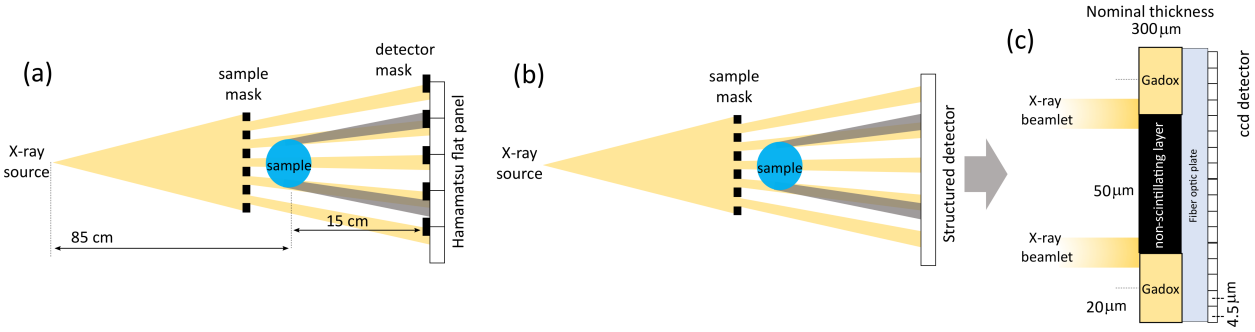

Figure 1: Panel (a) shows a schematic top view of an the edge illumination setup, employing two masks and a conventional flat panel detector. Panel (b) shows an edge illumination setup using the structured detector in combination with the sample mask only. Panel (c) illustrates the design of the detector employing the structured scintillator layer.

masks, as shown in Fig.1(a)[8,22]. The first mask, positioned in front of the sample and referred to as the sample mask, splits the main beam into a series of beamlets; these propagate to the detector where the second (detector) mask is aligned so as to intercept a portion of each. When a sample is inserted into the beam path, refraction causes a shift of the beamlets away from or towards the corresponding pixel, causing a decrease or an increase of the detected intensity, respectively. Through knowledge of the illumination curve (IC), the bell-shaped curve obtained in the absence of a sample by scanning the sample mask while the rest of the system is kept still, this change in intensity can be related directly to the refraction angle, which in turn depends on the decrement of the real part of the complex refractive index δ. In addition to refraction, the variation in beamlet intensity depends also on attenuation (related to the imaginary part of the refractive index, β). The disentanglement of these two quantities is referred to as phase retrieval, and requires the acquisition of more than one image at different relative mask positions (i.e. different positions on the IC)[23]. The conventional setup used in this work employed a Rigaku 007 rotating anode Molybdenum source featuring a focal spot size of 70 μm and operated at 40 kVp, 30 mA, located at about 85 cm from the detector[19,20]. The molybdenum anode provides a relative narrow energy bandwidth due to the dominance of the main emission lines at 17.5 and 19.6 keV. The detector, located at about 15 cm from the sample, was a Hamamatsu C9732DK flat panel with a pixel size of 50×50 μm^2 coupled with a detector mask having an aperture of 20 μm and period 98 μm. The sample mask is scaled according to the system's magnification. Both masks were manufactured by Creatv Microtech (Potomac, MD) and are made by gold electroplating on a 500 μm thick graphite substrate. This mask design is usually referred to as a "skipped" configuration, since one every other pixel column is not illuminated. This greatly reduces the cross-talk between pixels, improving the intrinsic spatial resolution of the detector[20,24]. However, multiple images acquired while shifting the sample in sub-period steps (referred to as dithering steps) have to be acquired and digitally recombined to access such an improved level of resolution, which is ultimately limited by the aperture size[25]. In the second EI system, the Hamamatsu detector and the detector masks were replaced by the "structured" detector described in the previous section (see Fig.1 (b) and (c)). System geometry and all the other system elements remained unchanged. To investigate the energy response of the detector, a tungsten anode operated at 50 kVp, providing a much wider spectrum compared to the Mo one, has also been used..

2.3 Sample preparation

To characterize the EI system based on the structured detector three different wires with different diameters made of aluminium, polyethylene terephthalate (PET) and polybutylene terephthalate (PBT) have been imaged. The same samples have been also imaged with the conventional EI system for comparison. To provide some proof-of-concept data on a prospective biomedical application (visualisation of cartilage in osteoarthritis), a chicken bone with a cartilage layer, fixed in formalin solution for 24h, has also been scanned with both the systems.

2.4 Data acquisition and analysis

When using the conventional EI system based on the Hamamatsu flat panel, 11 images have been acquired at different points of the IC for phase retrieval. For each point, 8 dithering steps have been acquired to achieve

aperture-limited resolution. An exposure time of 2 seconds per image was used. A similar acquisition scheme was followed with the structured detector, but acquiring 9 points on the IC with an exposure time of 45 seconds to compensate for the reduced efficiency compared to the conventional system. A careful design of all detector elements and their coupling, which was not undertaken in this case as our main goal was to prove the principle, is expected to reduce the gap in the detection of efficiency between the two systems. For both datasets, phase retrieval has been performed through a pixel-wise gaussian fit of the acquired illumination curve points. When using the structured detector, one beamlet covers more than one pixel. Prior to phase retrieval, all pixels hit by a certain beamlet were therefore summed up. The wire profiles acquired with both systems have been compared to the theoretical profiles obtained by means of a wave optics calculation, taking into account the polychromaticity of the spectrum, beam hardening, source and detector blurring and detector response[26]. For the detector response, the absorption coefficient of the scintillator material and its nominal thickness have been used. Having noticed some discrepancies in the energy response of the structured detector, namely an apparent oversensitivity to high x-ray energies, we performed a series of independent measurements using a Tungsten source operated at 40 kVp. Multiple exposures were acquired while filtering the spectrum with two different Al thicknesses (1 and 6 mm) as well as with no filtration, and the results compared to the expected intensity calculated as:

$$I \sim \int_0^{E_{max}} S(E) e^{-\mu_a t_a} (1 - e^{-\mu_g t_g}) E \cdot dE \tag{1}$$

where $S(E)$ is the spectral distribution and the integral extends from 0 up to $E_{max} = 40$ keV, μ_a,μ_g and t_a,t_g are the absorption coefficients and thickness for aluminium and gadox, respectively and the linear energy term E takes accounts for the integrating nature of the detector that makes it sensitive to the total energy deposited by the x-rays. To perform meaningful comparisons, data were normalized to the case where no filter was used.

3 Results and discussion

To demonstrate that refraction and transmission signals could be effectively retrieved from images obtained with the structured detector, and compare them to those obtained with a conventional EI system, wires of different materials have been acquired with both systems, and phase retrieval was applied to both datasets.

3.1 Quantitative response

The retrieved transmission images and corresponding line profiles for Aluminium, PET and PBT wires are shown in Fig.2. Specifically, Fig.2(a) shows images and profiles for the conventional EI system, demonstrating

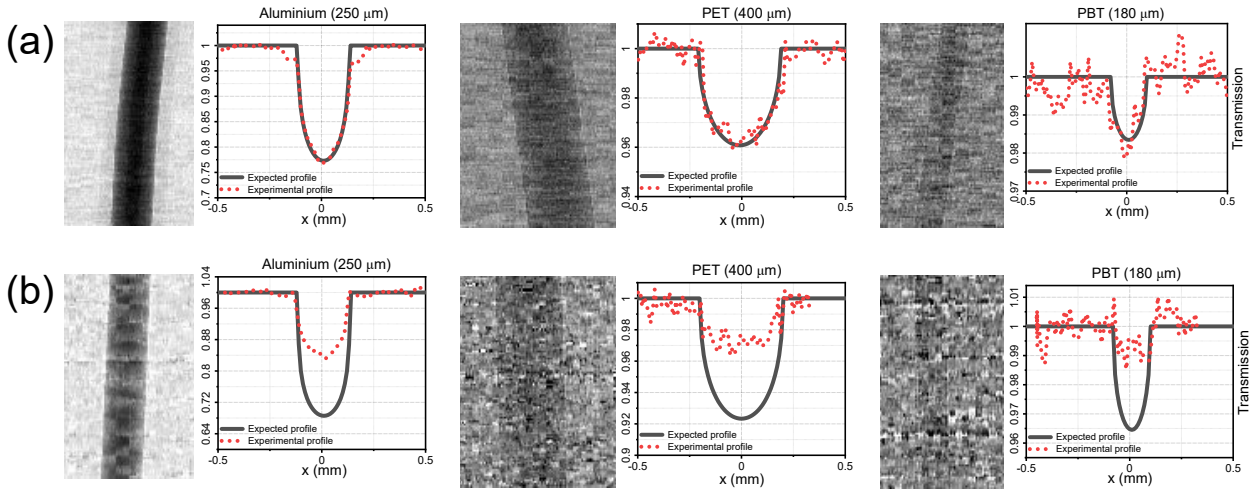

Figure 2: Panels (a) and (b) show the transmission images and associated experimental and theoretical line profiles for the edge illumination systems based on a flat panel and on the structured detector, respectively. From left to right materials are aluminium (250 μm diameter), PET (400 μm diameter) and PBT (180 μm diameter). In order to improve the line profiles, the average of 10 consecutive rows have been considered for aluminium and PET, while 20 rows have been considered for PBT.

a very good agreement between the simulated and experimental profiles for all materials. Conversely, the

profiles obtained from the structured detector (Fig.2(b)) exhibit a systematic underestimation of the expected absorption for all materials. In addition, a patchy appearance of the sample is evident in the image of the Al wire. This is attributable to a non-uniform filling of the scintillator layer, which introduces local variations in the detector energy sensitivity due to variations in the term t_{gdx} in eq.1. However, the underestimation of the transmission signal cannot be explained by local reductions in the scintillator thickness, since this would decrease the relative sensitivity to higher x-ray energies, leading to an overestimation of the sample transmission.

Similarly, the comparison of the refraction channels obtained with both EI systems are reported in Fig.3. Also in this case the line profiles extracted from the images acquired with a conventional EI system (see

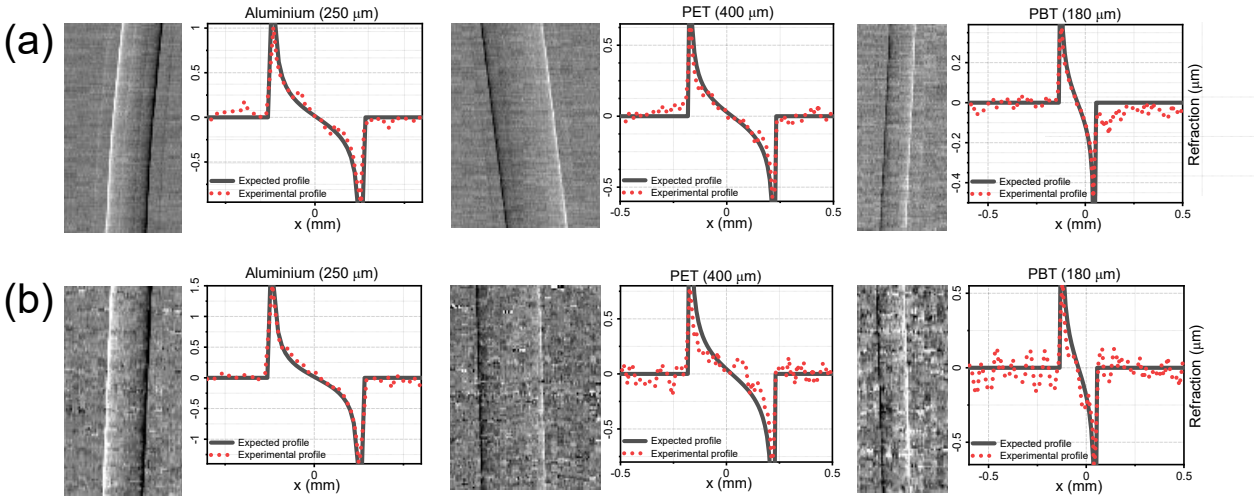

Figure 3: Similarly to Fig.2, panels (a) and (b) show the experimental and theoretical refraction line profiles for both the edge illumination systems. In particular, panel (a) is referring to the edge illumination system based on a conventional flat panel detector, while panel (b) to the one implementing the structured scintillator. Note that the top of the simulated refraction spectra has been intentionally left out to better highlight the mismatch in the central part of the wires, well visible especially for PET and PBT.

Fig.3(a)) show a very good agreement with the experimental ones. When the structured scintillator is used an underestimation of the refraction angle occurs, visible in the steeper trend in the central part of the wire. This result is in agreement with the trend observed in the transmission profile since the refraction angle decreases with increasing x-ray energy.

3.2 Energy response

To validate the hypothesis of a higher sensitivity of the structured detector to higher x-ray energies, a further test has been carried out. The transmitted intensity through different thicknesses of aluminium has been investigated for a tungsten X-ray spectrum. Results are reported in Fig.4. Specifically, panel (a) shows the comparison between the experimental intensity values detected using no filter and 1 and 6 mm of aluminium (black line), and the intensity values calculated through eq.1 (blue line) for the entire W spectrum shown in panel (b). All points have been normalised to the intensity obtained without the filter. The comparison between black and blue lines makes it evident that the transmission calculated in this manner is systematically underestimated at all considered thicknesses, suggesting a higher mean energy for the beam detected by the structured detector. In order to quantify this, the calculation of the expected transmitted intensity has been repeated while progressively cropping the lowest end of the W spectrum until the best match with the experimental data was observed, as indicated by the red line in panel (a). The spectrum leading to this result is indicated by the red sub-region in panel (b), and corresponds to the introduction of a sharp cut at 19 keV, leading to an average energy of 29.2 keV. For the avoidance of doubt, a sharp spectral cut is not expected to represent the real physical situation, but is merely a simplified means to demonstrate an increased sensitivity of the structured detector to higher x-ray energies. A similar analysis has been performed on the experimental images of the wires obtained with the structured detector. In this latter case the low-end of the molybdenum spectrum was cropped at increasing energies until the best match between simulated and experimental profiles was obtained; the resulting spectral cut and the residual differences between profiles are shown in Fig.4 (c) and (d), The "optimal" spectral cut has been obtained by minimizing the difference between simulated and experimental profiles for all materials and for both contrast channels. It is worth noting that, even if the Mo spectrum is significantly different from the W one and therefore an

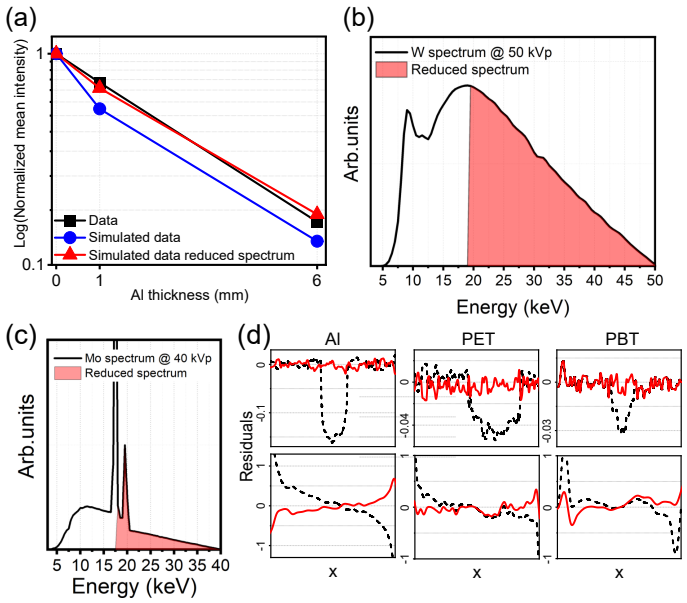

Figure 4: Panel (a) shows the experimental and calculated detected intensities for different Al filter thickness (0, 1 and 6 mm) and for entire and reduced W spectra. Panel (b) shows the spectra used to calculate the intensities shown in panel (a), with the entire spectrum and red portions used to calculate the points in the blue and red lines in panel (a), respectively. The latter minimises the difference between experimental and calculated intensities; a sharp cut of the spectrum has been used for simplicity's sake. Similarly, panel (c) shows the entire theoretical Mo spectrum and the reduced one (red area) obtained by minimizing the difference between the experimental and simulated profiles for all materials. The corresponding residuals are reported in panel (d) for transmission (top) and refraction (bottom). The solid red and dashed black lines show the difference between experimental and simulated profiles obtained using the reduced and the entire spectra, respectively.

exact match was not expected, a similar energy threshold has been found in the two cases. Specifically, a cut at 18 keV, producing an average energy of 23.7 keV, provided the best match between all profiles. However, even if these results demonstrate the qualitative observation of an oversensitivity to higher x-ray energies by the structured detector, the mechanism behind this effect requires further investigation. This is likely to be due to the excessive thickness of the scintillator layer, as mentioned above. This penalises the detection of low-energy x-rays because they are more likely to be stopped in the top gadox layer, and because they produce fewer visible photons. Generation of visible photons in the top layer means a higher re-absorption rate in the remaining gadox thickness, and a higher likelihood of hitting the walls of the apertures as they propagate towards the sensor. These two effects are exacerbated by the fact that fewer visible photons are produced in the first place.

3.3 Imaging application

Despite the suboptimal manufacturing process affecting its quantitative response, the structured detector was shown to be still capable of providing a sufficiently high image quality to visualize details which are typically invisible to conventional transmission. On top of the refraction images of low absorbing wires shown above, transmission and refraction images of a chicken bone obtained with both EI setups are shown in Fig.5; specifically, a region-of-interest focusing on the cartilage layer is shown. This is invisible in the transmission channel obtained with the structured detector (left hand side of panel (b)) while, due to the higher image quality produced by the uniform scintillator layer of the commercial detector, it is barely visible in the transmission channel on the left hand side of panel (a). On the other hand, the cartilage layer is clearly visible from the refraction images obtained with both systems, as indicated by the red arrows in the right hand side images of both panels. While image quality in the structured detector case is reduced by the discussed non-uniformity of the scintillator layer, one should also note that its sensitivity to higher effective x-ray energy E makes the detection of cartilage inherently more challenging, as the refraction angle scales with E^2; this notwithstanding, the edge of the cartilage is clearly detected. While in this case we have used a conventional phase retrieval method based on the acquisition of multiple images, the presented system is expected to be compatible with single image phase retrieval methods as already demonstrated for edge illumination[27], with a significant reduction of the scanning time, which is valuable especially for medical

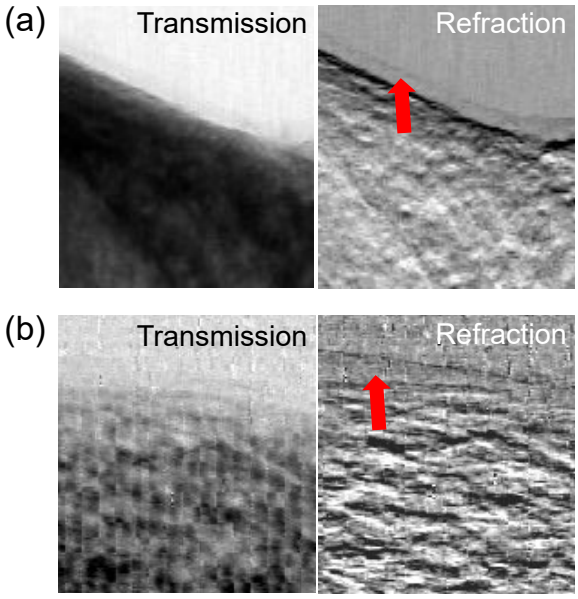

Figure 5: Panels (a) and (b) show transmission (left) and refraction (right) images of a chicken bone imaged with the conventional edge illumination system and the one based on the structured detector, respectively. The red arrows indicate the cartilage layer evident only in the refraction.

applications[10]. We also note that, while here we used a relatively high number of IC points to perform the retrieval, it was recently demonstrated that attenuation and refraction are particularly robust against a reduction of the number of points used for the retrieval[28].

4 Conclusions

This work presents the first proof-of-concept EI system in which the detector mask has been eliminated and replaced with a detector featuring a structured scintillator, allowing to effectively implement EI X-ray phase imaging with a single mask. We have shown that such a system allows to successfully retrieve the refraction channel in addition to conventional transmission, through which it was possible to visualizing features, such as cartilage, invisible in the latter. The unoptimized manufacturing process of the structured scintillator adopted for the first proof-of-concept test had adverse effects on image quality. In particular, a non-uniform filling of the apertures in the structured grid resulted in a patchy appearance of the images, which could be corrected for only in part through flat-fielding as it meant that each gadox-filled aperture had a slightly different energy response. The excessive thickness of the scintillator, chosen to ensure the creation of at least some signal in a situation where the degree of filling that could be expected was unknown, affected the quantitative response of the detector as it made it partially insensitive to low-energy x-rays. While further investigations are needed to improve the manufacturing process to obtain a high-quality detector for medical applications, this first pilot study indicates that the approach is viable. The system based on a single mask that could be developed through this approach would improve system stability, and could open the application of EI to rotating medical imaging devices.

Author Declarations

Piotr Dobrosz, Ed Bullard and Rob Brooks, Daniel Brau are, or were at the time the research was carried out, Scintacor and Photonic Science and Engineering employees, respectively.

Data Availability

The data that support the findings of this study are available from the corresponding author upon reasonable request.

Acknowledgement

This work was supported by EPSRC (grants EP/R511638/1 and EP/T005408/1). AO is supported by the Royal Academy of Engineering under their Chairs in Emerging Technologies scheme.

References

[1] A Snigirev, I Snigireva, V Kohn, S Kuznetsov, and I Schelokov. On the possibilities of x-ray phase contrast microimaging by coherent high-energy synchrotron radiation. Review of scientific instruments, 66(12):5486–5492, 1995.

[2] Atsushi Momose and Jun Fukuda. Phase-contrast radiographs of nonstained rat cerebellar specimen. Medical physics, 22(4):375–379, 1995.

[3] Bernd R Pinzer, M Cacquevel, Peter Modregger, SA McDonald, JC Bensadoun, T Thuering, P Aebischer, and Marco Stampanoni. Imaging brain amyloid deposition using grating-based differential phase contrast tomography. Neuroimage, 61(4):1336–1346, 2012.

[4] Merrick C Strotton, Andrew J Bodey, Kazimir Wanelik, Carl Hobbs, Christoph Rau, and Elizabeth J Bradbury. The spatiotemporal spread of cervical spinal cord contusion injury pathology revealed by 3d in-line phase contrast synchrotron x-ray microtomography. Experimental neurology, 336:113529, 2021.

[5] Marie-Christine Zdora, Pierre Thibault, Willy Kuo, Vincent Fernandez, Hans Deyhle, Joan Vila-Comamala, Margie P Olbinado, Alexander Rack, Peter M Lackie, Orestis L Katsamenis, et al. X-ray phase tomography with near-field speckles for three-dimensional virtual histology. Optica, 7(9):1221–1227, 2020.

[6] Lorenzo Massimi, Nicola Pieroni, Laura Maugeri, Michela Fratini, Francesco Brun, Inna Bukreeva, Giulia Santamaria, Valentina Medici, Tino Emanuele Poloni, Claudia Balducci, et al. Assessment of plaque morphology in alzheimer's mouse cerebellum using three-dimensional x-ray phase-based virtual histology. Scientific Reports, 10(1):1–10, 2020.

[7] Alberto Bravin, Paola Coan, and Pekka Suortti. X-ray phase-contrast imaging: from pre-clinical applications towards clinics. Physics in Medicine & Biology, 58(1):R1, 2012.

[8] Alessandro Olivo and Robert Speller. A coded-aperture technique allowing x-ray phase contrast imaging with conventional sources. Applied Physics Letters, 91(7):074106, 2007.

[9] Timm Weitkamp, Ana Diaz, Christian David, Franz Pfeiffer, Marco Stampanoni, Peter Cloetens, and Eric Ziegler. X-ray phase imaging with a grating interferometer. Optics express, 13(16):6296–6304, 2005.

[10] Lorenzo Massimi, Tamara Suaris, Charlotte K Hagen, Marco Endrizzi, Peter RT Munro, Glafkos Havariyoun, PM Sam Hawker, Bennie Smit, Alberto Astolfo, Oliver J Larkin, et al. Detection of involved margins in breast specimens with x-ray phase-contrast computed tomography. Scientific reports, 11(1):1–9, 2021.

[11] Ludovic Broche, Bertrand Favier, Hélène Rougé-Labriet, Sabine Drevet, Bernard Lardy, Emmanuel Brun, and Benjamin Lemasson. Calcified cartilage revealed in whole joint by x-ray phase contrast imaging. Osteoarthritis and Cartilage Open, 3(2):100168, 2021.

[12] Tilman Donath, Franz Pfeiffer, Oliver Bunk, Christian Grünzweig, Eckhard Hempel, Stefan Popescu, Peter Vock, and Christian David. Toward clinical x-ray phase-contrast ct: demonstration of enhanced soft-tissue contrast in human specimen. Investigative radiology, 45(7):445–452, 2010.

[13] Alberto Astolfo, Marco Endrizzi, Fabio A Vittoria, Paul C Diemoz, Benjamin Price, Ian Haig, and Alessandro Olivo. Large field of view, fast and low dose multimodal phase-contrast imaging at high x-ray energy. Scientific reports, 7(1):1–8, 2017.

[14] CK Hagen, PRT Munro, M Endrizzi, PC Diemoz, and A Olivo. Low-dose phase contrast tomography with conventional x-ray sources. Medical physics, 41(7):070701, 2014.

[15] Marco Endrizzi, Dario Basta, and Alessandro Olivo. Laboratory-based x-ray phase-contrast imaging with misaligned optical elements. Applied Physics Letters, 107(12):124103, 2015.

[16] Matthias Simon, Klaus Jürgen Engel, Bernd Menser, Xavier Badel, and Jan Linnros. X-ray imaging performance of scintillator-filled silicon pore arrays. Medical Physics, 35(3):968–981, 2008.

[17] Yang Du, Xin Liu, Yaohu Lei, Jinchuan Guo, and Hanben Niu. Non-absorption grating approach for x-ray phase contrast imaging. Optics express, 19(23):22669–22674, 2011.

[18] Lorenzo Massimi, Jeffrey A Meganck, Rebecca Towns, Alessandro Olivo, and Marco Endrizzi. Evaluation of a compact multi-contrast and multi-resolution x-ray phase contrast edge illumination system for small animal imaging. Medical Physics, 2020.

[19] Lorenzo Massimi, Charlotte K Hagen, Marco Endrizzi, Peter RT Munro, Glafkos Havariyoun, PM Sam Hawker, Bennie Smit, Alberto Astolfo, Oliver J Larkin, Richard M Waltham, et al. Laboratory-based x-ray phase contrast ct technology for clinical intra-operative specimen imaging. In Medical Imaging 2019: Physics of Medical Imaging, volume 10948, page 109481R. International Society for Optics and Photonics, 2019.

[20] Lorenzo Massimi, Tamara Suaris, Charlotte K Hagen, Marco Endrizzi, Peter RT Munro, Glafkos Havariyoun, PM Sam Hawker, Bennie Smit, Alberto Astolfo, Oliver J Larkin, et al. Volumetric high-resolution x-ray phase-contrast virtual histology of breast specimens with a compact laboratory system. IEEE Transactions on Medical Imaging, 2021.

[21] Glafkos Havariyoun, Fabio A Vittoria, Charlotte K Hagen, Dario Basta, Gibril K Kallon, Marco Endrizzi, Lorenzo Massimi, Peter Munro, Sam Hawker, Bennie Smit, et al. A compact system for intra-operative specimen imaging based on edge illumination x-ray phase contrast. Physics in Medicine & Biology, 64(23):235005, 2019.

[22] Marco Endrizzi, Fabio A Vittoria, Gibril Kallon, Dario Basta, Paul C Diemoz, Alessandro Vincenzi, Pasquale Delogu, Ronaldo Bellazzini, and Alessandro Olivo. Achromatic approach to phase-based multi-modal imaging with conventional x-ray sources. Optics express, 23(12):16473–16480, 2015.

[23] Marco Endrizzi and Alessandro Olivo. Absorption, refraction and scattering retrieval with an edge-illumination-based imaging setup. Journal of Physics D: Applied Physics, 47(50):505102, 2014.

[24] K Ignatyev, PRT Munro, RD Speller, and A Olivo. Effects of signal diffusion on x-ray phase contrast images. Review of Scientific Instruments, 82(7):073702, 2011.

[25] Paul C Diemoz, Fabio A Vittoria, and Alessandro Olivo. Spatial resolution of edge illumination x-ray phase-contrast imaging. Optics express, 22(13):15514–15529, 2014.

[26] Fabio A Vittoria, Paul C Diemoz, Marco Endrizzi, Luigi Rigon, Frances C Lopez, Diego Dreossi, Peter RT Munro, and Alessandro Olivo. Strategies for efficient and fast wave optics simulation of coded-aperture and other x-ray phase-contrast imaging methods. Applied optics, 52(28):6940–6947, 2013.

[27] PC Diemoz, CK Hagen, M Endrizzi, M Minuti, R Bellazzini, L Urbani, P De Coppi, and A Olivo. Single-shot x-ray phase-contrast computed tomography with nonmicrofocal laboratory sources. Physical Review Applied, 7(4):044029, 2017.

[28] Lorenzo Massimi, Tom Partridge, Alberto Astolfo, Marco Endrizzi, Charlotte K Hagen, Peter RT Munro, David Bate, and Alessandro Olivo. Optimization of multipoint phase retrieval in edge illumination x-ray imaging: A theoretical and experimental analysis. Medical Physics, 48(10):5884–5896, 2021.